Physicomechanical, Phase Composition, and *In Vitro* Study of High-Temperature Sintered ZTA/HA Composites

S.M. NAGA, M. SAYED, and H.F. EL-MAGHRABY

Recent research has reported the fabrication of highly dense bioceramic composites based on zirconia-toughened alumina (ZTA) and biogenic hydroxyapatite (HA). The influence of ZTA addition (in the range of 40 to 60 wt pct) on HA was studied and evaluated. X-ray diffraction (XRD) and scanning electronic microscope (SEM) analysis were used to investigate the phase composition and microstructure, while densification was evaluated by determining the apparent porosity and bulk density of the bodies according to ASTM C-20. The results revealed the formation of new phases, α-tricalcium phosphate (α-TCP), and hibonite ($CaAl_{12}O_{19}$), which developed as a result of the reaction between ZTA and HA. The produced phases improved the composites' sinterability and hence their mechanical properties. The addition of 50 wt pct ZTA is the optimal addition due to the resulting high mechanical strength: 179.62 ± 8 MPa, an excellent bioactivity which is promoted through the dissolution of α-TCP and the hydration of calcium aluminate phases.

https://doi.org/10.1007/s11661-019-05433-4

I. INTRODUCTION

THE great need for biocompatible materials with high mechanical properties has induced scientists to look for new materials. Bioceramics are currently treated as one of the most biomaterials which possess promising applications in the biomedical technology field.[1,2] Implanted bioceramics possessed the advantage of being compatible with the human body environment. Their biocompatibility is arising from their chemical composition, which includes ions commonly found in the physiological environment (such as Ca^{2+}, Mg^{2+}, K^{+}, Na^{+}, *etc*…).[3] Due to the excellent bioactivity and biocompatibility of hydroxyapatite and tricalcium phosphate (β-TCP), they are widely applied as bone substitute materials. The essential drawback of such materials is their unfavorable low mechanical strength, which restricts their application as a load-bearing bone substitute. To make such bioactive ceramics suitable for load-bearing bone repair applications, introducing of reinforcing material is preferred. ZrO_2, Al_2O_3, and zirconia-toughened alumina (ZTA) are excessively used to improve the mechanical properties of bioceramic materials due to their excellent mechanical properties.[4–10] The greatest disadvantage of ZrO_2 is its bioinert behavior, which might lead to the formation of a fibrous tissue layer surrounding the implant. Such a formed fibrous layer encourages debonding between the implant and the living tissue.[11,12] To overcome the abovementioned problem, either ZTA was coated with a bioactive material[13–18] or a composite formulated from ZTA/bioactive material was created.[19–25]

To prepare the nanohydroxyapatite (HA)/ZTA composite, nano-HA prepared by the precipitation method was mixed with different weight percentages of zirconia-toughened alumina (ZTA) powder prepared *via* the sol-gel technique. ZrO_2-Al_2O_3 powder was prepared by the colloidal procedure, which used the electrostatic force between the ZrO_2 sol and the Al_2O_3 starting material. The results showed that the addition of 15 wt pct ZA to nano-HA notably improved the bending strength, while the addition of 30 wt pct ZA reduced both the bending strength and the fracture toughness of the produced composite. The decrease in the bending strength and fracture toughness was attributed to the formation of tricalcium phosphate (TCP) and porosity, which resulted from the increase in the contact area between ZrO_2 and HA.[21]

ZTA powder fabricated by combined precipitation and calcined at 1250 °C was mixed with HA powder, fabricated *via* a wet chemical route, and either MgF_2 or CaF_2 as a source for fluorine to improve the sinterability of the prepared ZTA/HA composites. The results showed that with the increase in the HA content, the mechanical properties of the composite were enhanced.

S.M. NAGA, M. SAYED, and H.F. El-MAGHRABY are with the National Research Centre, Ceramics Department, El-Bohous Str., Dokki, Cairo 12622, Egypt. Contact email: monasayed382@yahoo.com
Manuscript submitted January 7, 2019.
Article published online August 23, 2019

The produced composites were bioactive, and composites that contained 30 wt pct of HA were the optimal compounds.[22]

The impact of alumina addition on the microstructure and sintering behavior of 20 pct fluoro- HA/80 pct ZrO_2 composites was studied by Smirnov *et al.*[25]They claimed that alumina addition decreased the sintering temperature to 1200 °C, prohibiting recrystallization and stabilizing t-zirconia.

Different proportions of Al_2O_3, ZrO_2, and TiO_2 were added to HA produced from calf femoral bone. HA was produced *via* the thermal treatment route through the calcination of bones at 850 °C for 4 hours to obtain pure HA free from the organic material of the bone. The well-mixed components were pressed and calcined at temperatures ranging between 900 °C and 1100 °C. The results indicated that the addition of alumina, zirconia, and titania improved the HA mechanical properties, as higher compressive strength and microhardness values were observed.[24]

Bioactive ceramics materials such as hydroxyapatite and tricalcium phosphate (β-TCP) have the ability to create a hydroxyl apatite layer when immersed in the simulated body fluid (SBF). The created artificial apatite layer is similar to the inorganic phase of natural human bones. The formed layer has the ability to bond with collagen fibrils and thus it is easily bonded with the bone when applied as an implant.[26,27] Moreover, the reaction between calcium phosphate and alumina or ZTA composites led to the creation of calcium aluminate phases. The produced calcium ions present in the calcium aluminate phases were responsible for bioactivity enhancement.[25] Furthermore, the above reaction produced TCP compounds, which encourage the formation of HAp nuclei *via* Ca and P ion dissociation.

In the current study, the reaction between a ZTA composite and biogenic HA at high firing temperatures offers potential advantages through the production of new phases, such as α-TCP and $CaAl_{12}O_{19}$, which have the ability to improve the bioactivity and mechanical properties. Natural HA produced from eggshells was used for the *in situ* formation of TCP/ZTA composites. To evaluate the produced composite, the sintering behavior, microstructure, mechanical properties, and biological behavior of the produced composite were studied.

II. MATERIALS AND METHODS

The materials used in the present study are nanohydroxyapatite (HA), synthesized in our laboratory from eggshell,[28] and ZTA composite[85 mol pct Al_2O_3/15 mol pct ZrO_2] prepared *via* the sol-gel technique.

A. *Synthesis of Zirconia-Toughened Alumina (ZTA) Powder*

Zirconia-toughened alumina (ZTA) was prepared in composition of 15 mol pct ZrO_2/85 mol pct Al_2O_3. First, 3 mol pct Y-PSZ was prepared by hydrolysis of zirconium (IV)-*n*-butoxide (STREM CHEMICALS) with the addition of yttrium nitrate (Y_2O_3 in HNO_3, STREM CHEMICALS). In another beaker, alumina was separately prepared by the hydrolysis of aluminum tri-isopropoxide, $Al_3(C_3H_7O)$ (Wessex Hous, Shaftesbury), with distilled water and a few drops of concentrated HNO_3 at 80 °C. To homogenize the solution, magnetic stirring was conducted for 2 hours. A small amount of nitric acid was added to the solution after cooling to guarantee complete hydrolysis. Then, 3 mol pct yttria-stabilized zirconia sol was added to the aluminum tri-isopropoxide solution to obtain a clear sol of ZTA. The resultant sol was aged overnight to form the gel. The formed gel was dried at 80 °C and then calcined at 1200 °C for 2 hours at a heating rate of 10 °C/min. Finally, the calcined gel was ground in a ball mill to pass a 90-mesh sieve.

B. *Fabrication of HA/ZTA Composites*

Different amounts of nano-HA powder were mixed thoroughly with calcined ZTA for 5 hours using a ball mill at a constant speed of 300 rpm for 2 hours. Zirconia balls were used as grinding media. The whole grinding process was carried out in a polypropylene container. Table I shows the batch compositions for pure HA and different ZTA/HA composites. The produced mixture was uniaxially pressed into discs of 15 mm diameter and ~ 6.0 mm thickness (for physical and microstructural characterization) and $60 \times 5 \times 5$ mm^3 rectangular bars (for the mechanical property investigation) under a pressure of 300 MPa. The formed samples were sintered in an electric oven with a static air atmosphere at 1500 °C, 1600 °C, 1625 °C, 1650 °C, and 1675 °C for 2 hours of soaking time at a 7 °C/min firing rate. Additionally, pure HA specimens were uniaxially pressed to the abovementioned dimensions and fired at 1200 °C, 1250 °C, 1275 °C, and 1300 °C for 2 hours. The batch composition of the study batches is shown in Table I.

C. *In Vitro Bioactivity Examination*

For the *in vitro* bioactivity study, the selected dense pure HA and composite samples (HZ50) were assessed by investigating the formation of an apatite layer on their surface. The studied samples were soaked in a simulated body fluid (SBF) under normal physiological conditions. The SBF was prepared using the same concentration and composition described by Kokubo and Takadama.[29] The samples were soaked in 100 mL SBF in polyethylene cups, which were maintained at 37 °C for 1, 3, 7, 14, 21, and 28 days at pH 7.4. A constant aliquot of the solution was collected at every desired time period for analysis of both calcium and phosphorus ion concentrations. The analysis was carried out using an inductively coupled plasma spectrometry (ICP) (Agilent ICP-OES 5100, Australia). After 28 days of immersion, the samples were removed from the SBF, gently washed with distilled water, and then dried at 37 °C for 1 hour. The dried samples were characterized by SEM and EDX [SEM; Model XL 30 (Philips,

Table I. Batch Compositions for Pure HA and Different ZTA/HA Composites

Batch Composition	HA, Wt Pct	ZTA, Wt Pct
HA	100	0
40ZTA	60	40
50ZTA	50	50
60ZTA	40	60

Eindhoven, Netherlands) attached with EDX unit analyses] to determine their bioactivity.

D. *Characterization of the Fabricated Composite*

1. *Physical, Microstructure and Phase Composition Analysis*

Archimedes' water immersion principle (ASTM C-20) was used to measure the sinterability parameters in terms of the apparent porosity and bulk density of the fabricated samples. Furthermore, the microstructure was examined through a scanning electron microscope (SEM, JEOL JSM-T20) with an attached energy-dispersive X-ray spectroscope (EDS) system for elemental analysis, which applied from a point on the polished cross-sections samples coated with a thin layer of gold. Phase composition of the prepared ZTA composite, as well as of *in situ* calcium phosphate/ZTA composite samples, were evaluated using an X-ray diffraction apparatus (Philips, PW 1730 X-ray diffractometer) with a Cu Kα target and a secondary monochromator Ni filter.

2. *Mechanical Property Evaluation*

The three-point bending strength was measured using a universal testing machine (Model 4204, Instron Corp., Danvers, MA) at a crosshead speed of 0.5 mm/min and a support distance of 40 mm. The compressive strength was measured using a universal hydraulic testing machine [Shimadzu 3000 KN, Japan]. Ten specimens were measured for each data point.

III. RESULTS

A. *Physical Properties*

The HA and studied composite batches fired at different sintering temperatures were tested for bulk density and apparent porosity. The results recorded for pure HA and fabricated composite samples, shown in Figures 1(a), 2(a) and (b), respectively. The sintering behavior of the pure hydroxyapatite in Figure 1(b) indicated that the increase in sintering temperature from 1200 °C to 1275 °C led to lower apparent porosity and improved bulk density, Figure 1(a). A further increase in the sintering temperature up to 1300 °C increased the apparent porosity and decreased the bulk density, Figure 1(b).

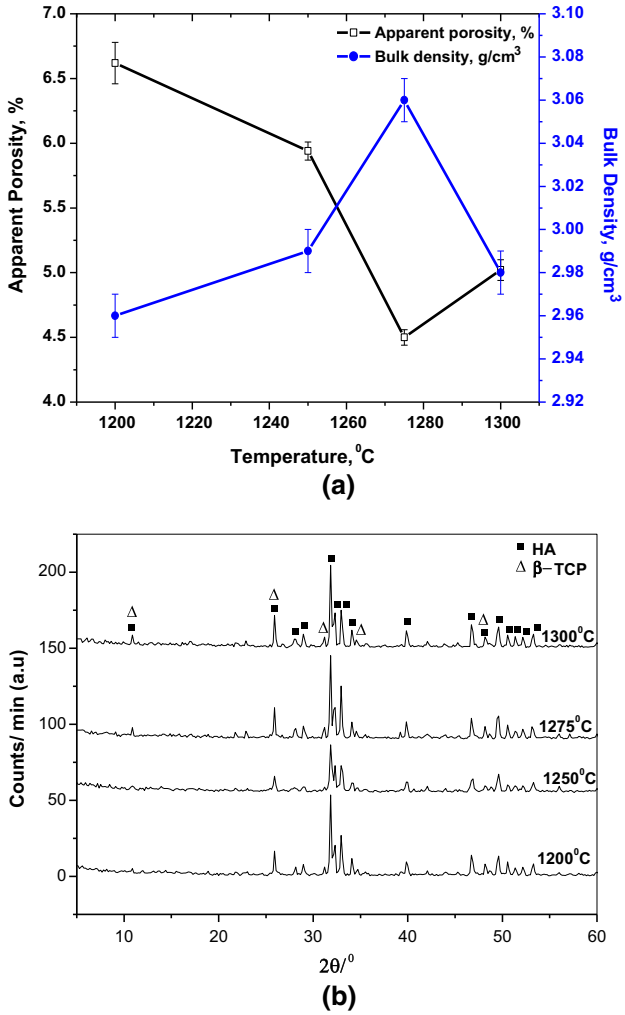

Fig. 1—Physical properties (*a*) and XRD patterns (*b*) of the pure HA dense bodies sintered at different firing temperatures for 2 h.

On the other hand, the results revealed that the increase in the ZTA content increased the sintering temperature of the composites containing ZTA. The detected optimum sintering temperature was increased from 1275 °C for pure HA to 1600 °C for 40 mass pct ZTA specimens, and 1625 °C for 50 and 60 mass pct ZTA specimens. All the samples are soaked for 2 hours at their optimum sintering temperature, Figures 2(a) and (b).

B. *Phase Composition*

The phase composition analysis of pure ZTA, 40ZTA, 50ZTA, and 60ZTA composite samples sintered at their optimum sintering temperature at 1650 °C for pure ZTA, 1600 °C for 40 wt pct ZTA specimens, and 1625 °C for 50 and 60 wt pct ZTA specimens is illustrated in Figure 3. It was observed that alumna (Al_2O_3) and m-zirconia (m-ZrO_2) phases were the only components of the pure ZTA composite fired at 1650 °C. In contrast, the addition of various amounts of ZTA (40, 50, and 60 wt pct) to the HA composites led to the formation of α-TCP and hibonite phases. When firing at

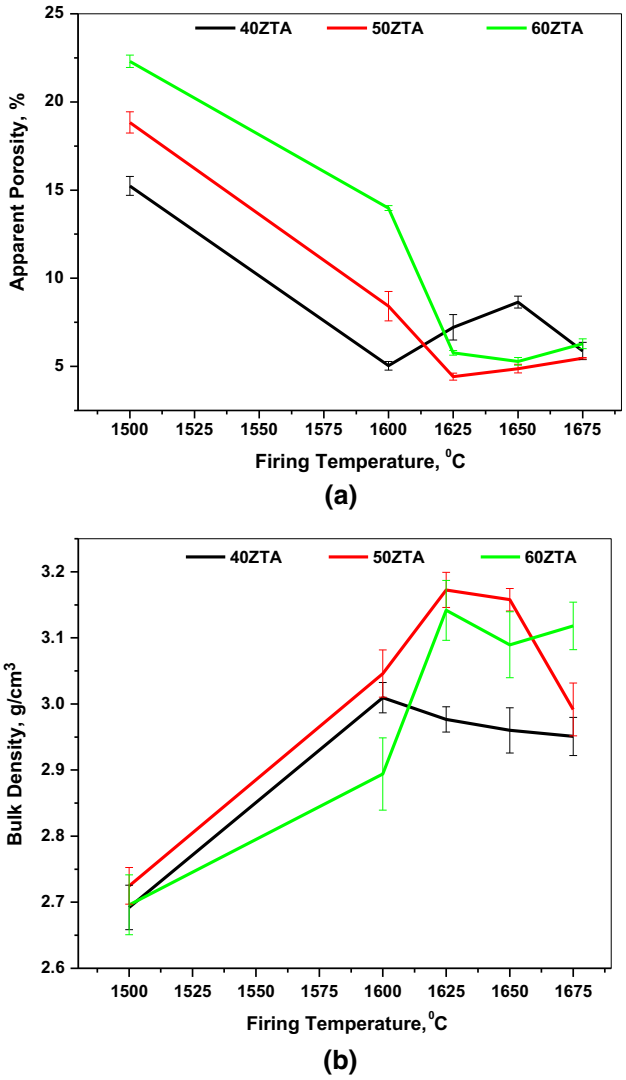

Fig. 2—Physical properties of ZTA/HA composites sintered at different sintering temperatures (*a*) apparent porosity and (*b*) bulk density.

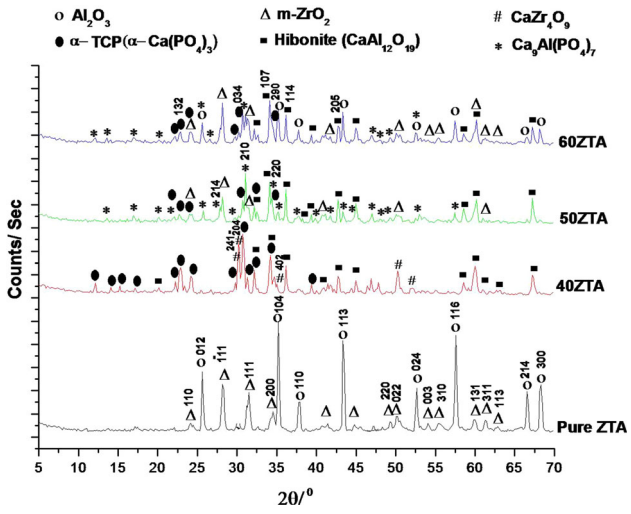

Fig. 3—XRD patterns of pure ZTA, 40ZTA, 50ZTA, and 60ZTA composites sintered at their optimum sintering temperature for 2 h.

high temperatures, HA decomposes into TCP, and CaO is released.

The released CaO reacts with alumina to form the hibonite phase, $CaAl_{12}O_{19}$. $CaZr_4O_9$ was observed in the 40ZTA composite only. The 50ZTA and 60ZTA composites exhibited α-TCP, hibonite, alumina, zirconia, and calcium aluminum phosphate [$Ca_9Al(PO_4)_7$] phases. The XRD data of the formed Al_2O_3, m-ZrO_2, $CaZr_4O_9$, α-TCP, $CaAl_{12}O_{19}$, and $Ca_9Al(PO_4)_7$ phases were identical to the ICDD (JCPDS) standard cards (42-1468, 37-1484, 80-1342, 70-0364, 76-0665, and 48-1192, respectively).

C. *Microstructure*

An SEM micrograph of the polished pure HA samples fired at 1275 °C is given in Figure 4(a). The figure indicates that the samples exhibited a bimodal distribution of grains, and there is almost no evidence of pores. This result reinforced the findings obtained from the sintering results, which showed that HA samples sintered at 1275 °C are dense bodies possessing a high relative density of 96.95 pct.

The SEM micrograph for pure ZTA samples [Figure 4(b)] showed that zirconia particles were homogeneously distributed either as agglomerate batches or as small particles present at the triple junction of alumina particles (intergranular) or within the alumina particles (intragranular). Figure 4(c) confirms the presence of hibonite in the 40ZTA samples. Hexagonal hibonite particles were present in batches within the α-TCP matrix, while zirconia particles were present as small white spheres. With the increase in ZTA content up to 50 and 60 pct and the reduction in HA content, a new phase [$Ca_9Al(PO_4)_7$] developed. The newly developed phase appeared in the form of husks, as observed in Figure 4(d). Alumina, α-TCP, m-ZrO_2, and hibonite were also observed. The ZrO_2 particles present in the 60ZTA composite were coarser than those in 40ZTA composites. EDS patterns confirmed the formation of hibonite, $Ca_9Al(PO_4)_7$, and α-TCP. In contrast, detection of the formation of $CaZr_4O_9$, either by SEM or EDS, was difficult. The abovementioned results agree with the XRD results (Figure 3).

D. *Mechanical Properties*

The mechanical properties in terms of compressive and bending strength were studied for pure HA sintered at 1275 °C, and fabricated composited sintered at 1600 °C for 40 wt pct ZTA specimens, and 1625 °C for 50 as well as 60 wt pct ZTA specimens for 2 hours, as demonstrated in Figure 5. The addition of ZTA to HA boosted the compressive and bending strengths of the produced composite. An increase in the ZTA content up to 60 pct reduced the composite's mechanical properties, as shown in Figure 5. The obtained compressive strength value for the fabricated 50 pct ZTA/HA composite was 179.62 ± 8 MPa, which is within the range of the human Cortical bones' compressive strength.[30]

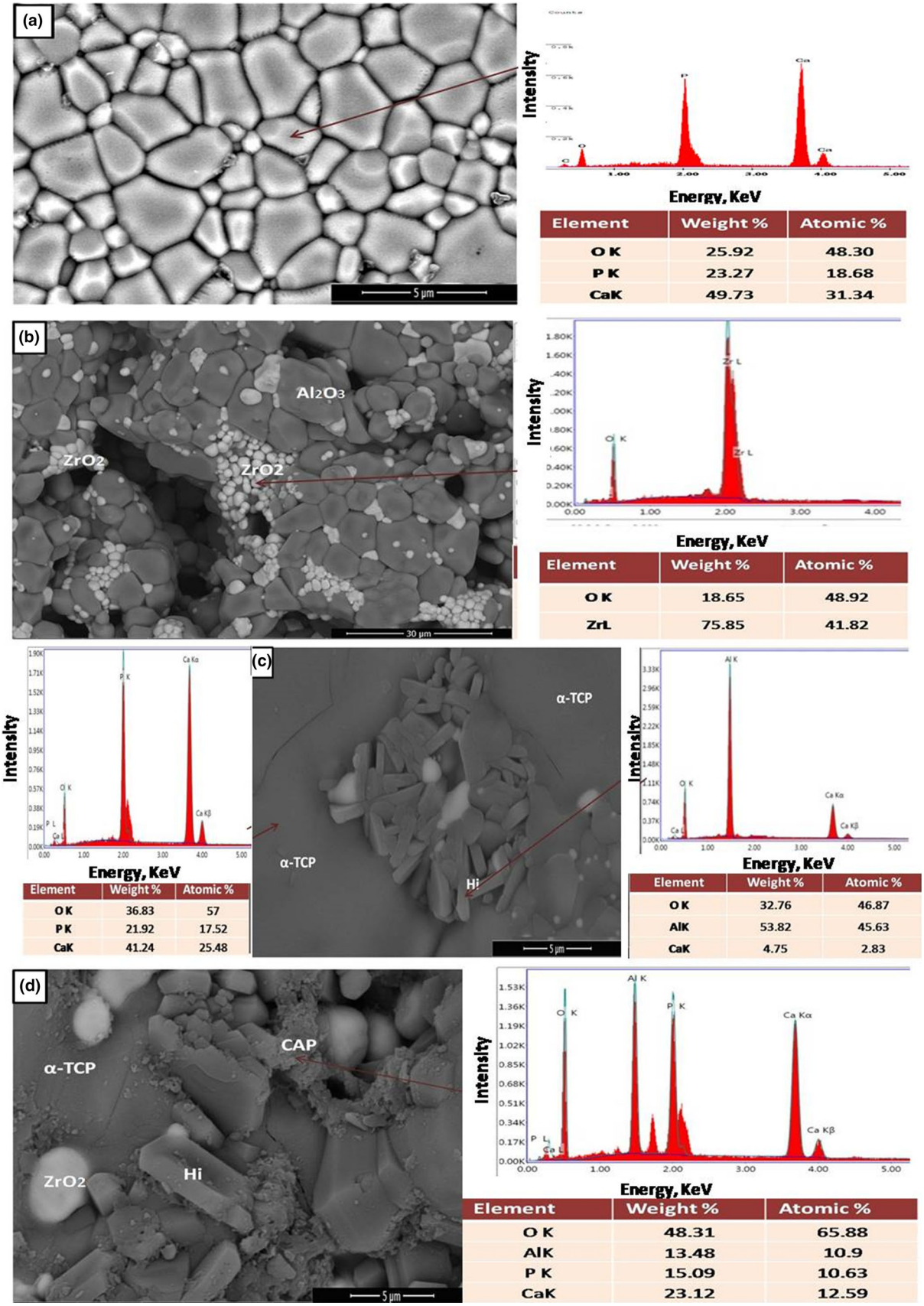

Fig. 4—Scanning electron microscopy (SEM) and energy dispersion XRD spectroscopy (EDX) of (*a*) pure HA, (*b*) pure ZTA, (*c*) 40ZTA composite and (*d*) 60ZTA composite at their optimum sintering temperature.

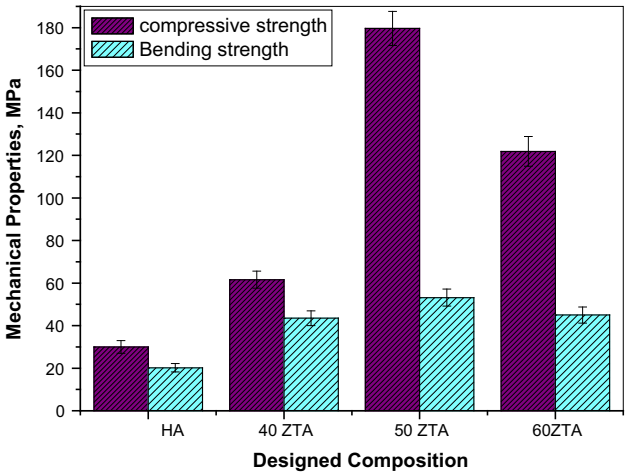

Fig. 5—The compressive and bending strengths of the pure HA and the fabricated composites sintered at their optimum sintering temperature for 2 h.

E. *Bioactivity Measurements, In Vitro Test of Dense HA, and 50 Pct ZTA/HA Composites*

The abovementioned results indicated that 50ZTA composites possess the optimum physical and mechanical properties. Hence, bioactivity measurements were carried out for pure HA and 50ZTA dense bodies sintered at 1625 °C for 2 hours. Table II displays the relationships of the mean concentrations of Ca^{2+} and PO_4^{3-} ions (mg/L) and pH measurements with the incubation time in the SBF solution. The results showed that the Ca^{2+} ion content for pure HA decreased throughout the whole experiment period. The PO_4^{3-} ion content showed an increase after the first week and then the concentration decreased gradually till the end of the experiment. 50ZTA composites showed a decrease in the Ca^{2+} content in the first 2 weeks, followed by an increase in the Ca^{2+} concentration. On the other hand, 50 pct ZTA/HA showed a decrease in the PO_4^{3-} content, followed by an increase during the remaining 3 weeks. The results showed that the Ca^{2+} ion decreased from 98.74 to 57.62 (mg/L), and PO_4^{3-} ion contents slightly increased from 32.62 to 38.11 (mg/L) for pure HA after 28 days of immersion in SBF.

The SEM micrographs of HA after immersion in SBF solution and the 50ZTA composite sample before and after incubation in SBF solution for 28 days are shown in Figures 6(a) through (c), respectively. Figure 6(a) shows a rough surface, which is completely different from the initial surface shown in Figure 4(a). HA deposited from SBF solution was present as crust-like precipitates. The figure depicts coarse flaky particles as well as fine spherical particles. Figure 6(a) clearly shows the presence of fine particles, which may be due to the presence of carbonate ions. An increase in carbonate concentration decreases the HA size.[31] The presence of Ca^{2+}, PO_4^{3-}, and C^{2+} ions was confirmed by EDS analysis of the newly formed HA crystals. The wt pct of P, Ca, O, and C were 22.63, 46.53, 24.76, and 6.08, respectively.

Figures 6(b) and (c) illustrate the SEM micrographs of the 50ZTA scaffold samples before and after immersion in SBF solution for 28 days. The alteration of the surface morphology for 50ZTA samples before and after incubation in SBF solution Figures 6(b) and (c) indicate the formation of newly HA particles confirmed through EDS analysis.

IV. DISCUSSION

Development of new bioceramic materials that possess high mechanical and bioactivity properties has become a great challenge in biomedical field for load-bearing application. In the present study, we fabricated bioceramic composites based on the combination of high content ZTA (40 to 60 wt pct) and bioactive HA derived from eggshell at high firing temperatures. It was found that sintering of the pure hydroxyapatite in sintering temperature ranging between 1200 °C and 1275 °C lowered the apparent porosity and improved the bulk density. However, increasing the sintering temperature up to 1300 °C led to increased apparent porosity and decreased bulk density, Figure 1(a). This phenomenon is attributed to the beginning of partial decomposition of hydroxyapatite into the β-TCP phase at 1300 °C [Figure 1(b)].[32]

On the other hand, the addition of ZTA increased the sintering temperature due to the high melting points of Al_2O_3 and ZrO_2 (2060 °C and 2700 °C, respectively) in comparison to HA (1670 °C). The obtained results agree with those achieved by Afzal *et al.*[33] Moreover, the different phases developed after firing had a great influence on the densification behavior of the specimens. The XRD pattern, shown in Figure 3, indicated the formation of α-TCP and hibonite phases, as well as ZrO_2 and Al_2O_3. α-TCP and hibonite possess relatively low density in comparison to ZrO_2 and Al_2O_3 (Figure 3). Accordingly, with the increase in the HA content, more low-density phases will be formed, and it is logical to note a decrease in the bulk density.

The presence of Tricalcium phosphate is associated with the nature of HA instability in the presence of zirconia under high-temperature sintering. The transformation process proceeds according to the following equations[34]:

$$Ca_{10}(PO_4)_6(OH)_2 \rightarrow 3Ca_3P_2O_8 + H_2O + CaO.$$

When firing at high temperatures, HA decomposes into TCP and CaO is released. The released CaO reacts with alumina to form the hibonite phase, $CaAl_{12}O_{19}$,[35,36] according to the following equation[37]:

$$CaO + 6Al_2O_3 \rightarrow CaAl_{12}O_{19}.$$

In some cases, the released CaO is consumed in the reaction with zirconia to form $CaZrO_3$ or c-ZrO_2, the reaction proceeds according to the following equation.[38] However, $CaZr_4O_9$ was observed only in the 40ZTA composite at high firing temperature 1600 °C

Table II. The Mean Values of Ca^{2+} and PO_4^{3-} Ions (mg/L), pH Measurement Against the Incubation Time in the SBF Solution for Pure HA and 50ZTA Composite

	Ca^{2+} (mg/L)		PO_4^{3-} (mg/L)		pH Measurement	
Time	Pure HA	50ZTA	Pure HA	50ZTA	Pure HA	50ZTA
Initial Time	98.74	98.74	32.62	32.64	7.45	7.45
1W	75.23	93.24	41.61	30.82	8.26	7.23
2W	71.14	97.23	39.11	40.71	8.10	7.71
3W	67.42	99.12	38.03	41.40	8.54	7.74
4W	57.62	102.57	38.11	41.55	8.72	7.76

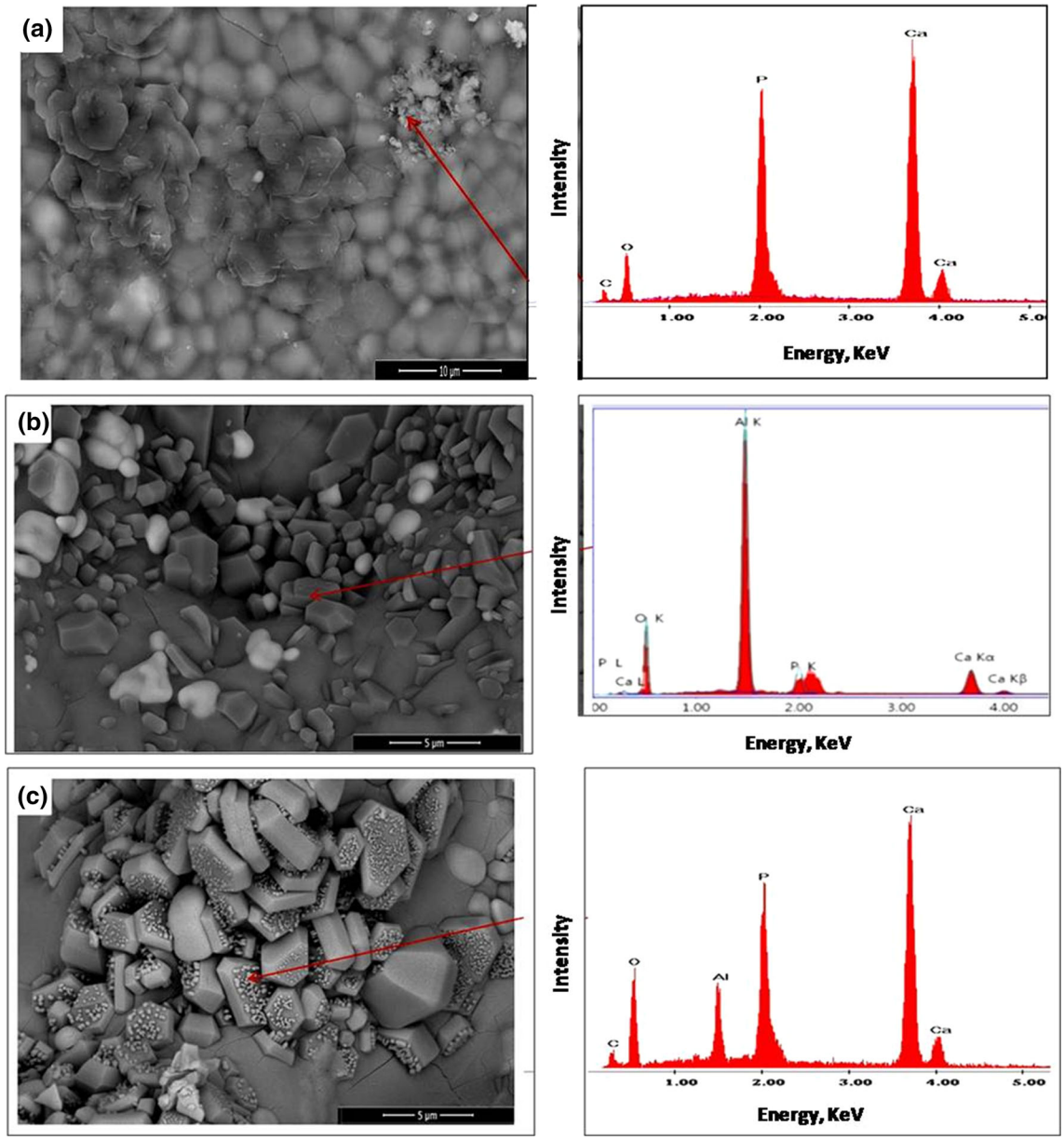

Fig. 6—SEM micrographs and energy dispersive XRD spectra (EDS) of pure HA after immersed in SBF solution (*a*); and 50ZTA composite before incubation in SBF solution (*b*) and after immersed in SBF solution for 28 days (*c*).

and it was absent in the other composites. The high content of HA in the 40ZTA composite in comparison to that in the other composites led to an increase in the CaO released during the decomposition of HA and accordingly enabled $CaZr_4O_9$ formation

$$CaO + m\text{-}ZrO_2 \rightarrow CaZrO_3 \text{ or } c\text{-}ZrO_2.$$

The 50ZTA and 60ZTA composites exhibited α-TCP, hibonite, alumina, zirconia, and calcium aluminum phosphate [$Ca_9Al(PO_4)_7$] phases. $Ca_9Al(PO_4)_7$ is thought to form as a result of the reaction between TCP and alumina.[39]The SEM and EDS results agree with the XRD results (Figure 3).

The reduction in the mechanical properties with the increase in ZTA content up to 60 pct is attributed to the influence of alumina and ZTA on HA at high sintering temperature, Figure 5. It is well known that the addition of alumina and ZTA and an increase in the sintering temperature reduce the mechanical properties of HA because of the formation of TCP phases and the liberation of CaO, as well as the increase in the sintered body's pore content.[40–42] In our case, there were three factors that influenced the mechanical properties. The first factor was the decrease in porosity. The reduced porosity of the sintered composites containing 50 pct ZTA enhanced the mechanical properties. On the other hand, the relatively higher porosity of the bodies containing 40 and 60 pct ZTA lessened the mechanical properties. The porosity reduction of the 50 pct ZTA composites improved the mechanical properties in terms of crushing and bending strength by maximizing the resistance of the bodies to applied loads.[43,44] The second factor was the formation of the hibonite phase. Hannora[45] mentioned that the formation of hibonite enhanced the mechanical properties of HA/alumina composites, in agreement with our recent results. In contrast, with an increase in the alumina content, the mechanical properties were reduced. This phenomenon may be due to the formation of weak bonding between alumina and the calcium aluminum phosphate phase. The remaining alumina and zirconia particles had a great influence on the improvement of the mechanical properties. The third factor was the presence of both ZrO_2 and Al_2O_3 particles. The increase in the ZTA content up to 50 pct enhanced the mechanical properties, but a further increase in the ZTA content up to 60 pct decreased both the bending and compressive strengths of the bodies. We believe that this phenomenon is due to the extreme reaction between HA and ZrO_2 to form TCP and m-ZrO_2.[21]

The change in the Ca^{2+} and PO_4^{3-} ion concentrations indicated the consumption of Ca^{2+} and PO_4^{3-} ions from the solution for the formation of a calcium phosphate layer on the surface of HA bodies, Table II. After the first week of 50ZTA composite immersion in SBF, both the Ca^{2+} and PO_4^{3-} ion concentrations decreased. Such ion concentration reduction confirmed the early formation of the apatite phase on the surface of the 50ZTA composite. The pH measurements confirmed the abovementioned conclusions. The pH value decreased from 7.40 to 7.23 during the first week of immersion for the 50ZTA composite, which indicated the early formation of the apatite phase. Later, and during the second week up to the fourth week, the pH value increased, which suggested the dissolution of α-TCP.[46] The bioactivity measurements for 50ZTA composites emphasize that the dissolution of α-TCP and the hydration of calcium aluminate phases during the incubation of the samples in SBF solution are responsible for the formation of the apatite phase on the surface of the scaffolds. α-TCP dissolution generated Ca^{2+} and PO_4^{3-} ions, which enhanced the formation and deposition of apatite on the surface of the 50ZTA composite,[47] while calcium aluminate compound dissociation produced Ca^{2+}, $Al(OH)_4^-$, and OH^- ions at the surface of 50ZTA composites. The presence of Ca^{2+} and PO_4^{3} ions produced from the dissolution of the α-TCP phase and the OH^- ions generated from the dissolution of calcium aluminate promoted the formation and precipitation of apatite grains, as illustrated in the following equation.[48]

$$5Ca^{2+} + 3PO_4^{3-} + OH^- \rightarrow Ca_5(PO_4)_3(OH).$$

Comparison between Figures 6(b) and (c) for 50ZTA composites clearly indicated the formation of HA particles on the surface of the 50ZTA composites. The EDS analysis of the newly formed HA phase revealed high percentages of Ca^{2+} and PO_4^{3-} ions in comparison to the 50ZTA composite sample analysis before immersion in SBF solution, which confirmed the formation of the new HA phase.

In our study, we introduce novel bio-composites based on the combination high content of ZTA and biogenic HA to produce sintered bodies having adequate mechanical strength for load-bearing applications. The HA used is fabricated from natural resources that contain in their composition valuable elements necessary for bone formation.[49] The other published articles[21,22,24,25] are based on HA prepared from chemical resources. Our produced bioceramics has many advantages such as recycling and reuse eggshells biowaste as promising natural resource in the production of inexpensive valuable bioceramic materials. The mechanical strength in terms of compressive and bending strength achieved in pervious study was 23.1 and 24.99 MPa, respectively [for 20-mass pct ZTA/HA composites sintered at 1275 °C],[50] while the mechanical strength in the present study was improved to reach 179.62 and 53.34 MPa for compressive and bending strength, respectively [for 50-mass pct ZTA/HA composite samples sintered at 1625 °C]. This improvement was achieved through applying high sintering temperatures enough for the full sintering of the composites, as well as addition of high mass-percent of ZTA to biogenic HA.

V. CONCLUSIONS

1. In this study, novel bioceramic scaffolds based on the combination of high content ZTA and biogenic

HA produced from the eggshell. The sintering of ZTA and HA at high temperature provides a bioceramic material with an *in vitro* ability to form HA at its surface together with approved mechanical properties for high load application.

2. α-TCP and hibonite phases are formed as a result of high-temperature sintering of HA/ZTA composites.
3. The formation of $CaZr_4O_9$ in the 40ZTA composite is attributed to its high HA content in comparison to the other composites. The higher HA content led to the increase in CaO released during the decomposition of HA and accordingly enabled $CaZr_4O_9$ formation.
4. The improvement in the mechanical behavior of the sintered composites is due to the reduction in the porosity content, the formation of the hibonite phase, and the presence of residual alumina and zirconia particles.
5. The dissolution of α-TCP and the hydration of calcium aluminate phases during incubation in SBF solution produced Ca^{2+} and PO_4^{3-} as well as OH^- ions. The presence of such ions promoted the formation and precipitation of apatite grains on the surface of the studied composites.

CONFLICT OF INTEREST

The authors declare that they have no conflict of interest.

REFERENCES

1. L.L. Hench: *J. Am. Ceram. Soc.*, 1998, vol. 81 (7), pp. 1705–28.
2. L.L. Hench and J. Wilson: *Series in Ceram*, World Scientific Publishing, Singapore, 1993, vol. 1.
3. M. Wang: *Biomaterials*, 2003, vol. 24, pp. 2133–51.
4. A.H. De Aza, J. Chevalier, G. Fantozzi, M. Schehl, and R. Torrecillas: *Biomaterials*, 2002, vol. 23, pp. 937–45.
5. B. Basu, J. Vleugels, and O. Van Der Biest: *J. Alloys Compds.*, 2004, vol. 365 (1–2), pp. 266–70.
6. C. Piconi, W. Burger, H.G. Richter, A. Cittadini, G. Maccauro, V. Covacci, N. Bruzzese, G.A. Ricci, and E. Marmo: *Biomaterials*, 1998, vol. 19 (16), pp. 1489–94.
7. R. Stevens: *Trans. Br. Ceram.*, 1981, vol. 80, pp. 81–85.
8. C. Pecharromán, J.F. Bartolomé, J. Requena, J.S. Moya, S. Deville, J. Chevalier, G. Fantozzi, and R. Torrecillas: *Adv. Mater.*, 2003, vol. 15, pp. 507–11.
9. A.K. Pandey, U.R. Jena, and K. Biswas: *Mater. Chem. Phys.*, 2014, vol. 146, pp. 456–63.
10. O. Roualdes, M.E. Duclas, D. Gutknecht, L. Frappart, J. Chevalier, and D.J. Hartmann: *Biomaterials*, 2010, vol. 31, pp. 2043–54.
11. J.R. Kelly and I. Denry: *Dent. Mater.*, 2008, vol. 24, pp. 289–98.
12. M. Hisbergues, S. Vendeville, and P. Vendeville: *Mater. Res. Part B Appl. Biomater.*, 2009, vol. 88, pp. 519–29.
13. J. Pierri, E.B. Roslindo, R. Tomasi, E.M.J. Agnolon Pallone, and E.C.S. Rigo: *J. Non-Cryst. Solids*, 2006, vol. 35, pp. 5279–83.
14. H. Esfahani, A. Nemati, and E. Salahi: *J. Adv. Appl. Ceram Struct. Funct. Biol. Ceram.*, 2013, vol. 112, pp. 140–45.
15. A. Rapacz-Kmita, A. Ślósarczyk, and Z. Paszkiewicz: *Ceram. Int.*, 2005, vol. 31, pp. 567–71.
16. R. Sultana, J. Yang, Z. Sun, and X. Hu: *J. Ceram. Sci. Technol.*, 2017, vol. 8, pp. 265–76.
17. K. Schickle, J. Spitz, S. Neuss, and R. Telle: *J. Eur. Ceram. Soc.*, 2018, vol. 38, pp. 271–77.
18. T.A.I. Sartori, J.A. Ferreira, D. Osiro, L.A. Colnago, and E.M.A. Pallone: *J. Eur. Ceram. Soc.*, 2018, vol. 38, pp. 743–51.
19. Y.M. Kong, C.J. Bae, S.H. Lee, H.W. Kim, and H.E. Kim: *Biomaterials*, 2006, vol. 26, pp. 509–17.
20. K.A. Khalil and S.W. Kim: *Mater. Sci. Forum*, 2007, vols. 534–536, pp. 1033–36.
21. I. Mobasherpour, M. Solati Hashjin, S.S. Razavi Toosi, and R. Darvishi Kamachali: *Ceram. Int.*, 2009, vol. 35, pp. 1569–74.
22. V.K. Singh and B.R. Reddy: *Ceram. Int.*, 2012, vol. 38, pp. 5333–40.
23. M.A.F. Afzal, P. Kesarwani, K.M. Reddy, S. Kalmodia, B. Basu, and K. Balani: *Mater. Sci. Eng. C*, 2012, vol. 32, pp. 1164–73.
24. I. Ozden, M. Ipekoglu, N. Mahmutyazicioglu, and S. Altintas: *Key Eng. Mater.*, 2011, vols. 493–494, pp. 199–204.
25. S.H. Oh, S.Y. Choi, Y.K. Lee, K.N. Kim, and S.H. Choi: *J. Biomed. Mater. Res. Part A*, 2003, vol. 67A (1), pp. 104–11.
26. G. Thrivikraman, G. Madras, and B. Basu: *RSC Adv.*, 2014, vol. 4, pp. 12763–81.
27. P. Kumar, B.S. Dehiya, and A. Sindhu: *Int. J. Appl. Eng. Res.*, 2018, vol. 13 (5), pp. 2744–52.
28. M. Sayed, H.F. El-Maghraby, F. Bondioli, and S.M. Naga: *J. Appl. Pharm. Sci.*, 2018, vol. 8 (03), pp. 023–30.
29. T. Kokubo and H. Takadama: *Biomaterials*, 2006, vol. 27, pp. 2907–15.
30. A.J.W. Johnson and B.A. Herschler: *Acta. Biomater.*, 2011, vol. 7, pp. 16–30.
31. X. Han and D.E. Day: *J. Mater. Sci: Mater. Med.*, 2007, vol. 18, pp. 1837–47.
32. M. Sayed: Environmental friendly preparation and characterization of biogenetic hydroxyapatite composites. PhD. Thesis, *University of Ain Shams*, 2016.
33. M.A.F. Afzal, P. Kesarwani, K.M. Reddy, S. Kalmodia, B. Basu, and K. Balani: *Mater. Sci. Eng. C*, 2012, vol. 32, pp. 1164–73.
34. I. Mobasherpour, M. Solati Hashjin, S.S. Razavi Toosi, and R. Darvishi Kamachali: *Ceram. Int.*, 2009, vol. 35, pp. 1569–74.
35. L. Xu, Z. Xie, L. Gao, X. Wang, F. Lian, T. Liu, and W. Li: *Ceram. Int.*, 2005, vol. 31, pp. 953–58.
36. M.H.F. Xue, Y. Liu, Y.G. Liu, D.X. Yang, D.Y. Ye, and Z.H. Huang: *Key Eng. Mater.*, 2012, vols. 512–515, pp. 539–42.
37. K. Vishista: *J. Am. Ceram. Soc.*, 2005, vol. 88 (5), pp. 1175–79.
38. J.M. Wu and T.S. Yeh: *J. Mater. Sci.*, 1988, vol. 23 (10), pp. 3771–77.
39. A.E. Hannora: *J. Ceram. Sci. Technol.*, 2014, vol. 05 (04), pp. 293–98.
40. S.J. Kim, H.G. Bang, J.H. Song, and S.Y. Park: *Ceram. Int.*, 2009, vol. 35, pp. 1647–50.
41. H.W. Kim, Y.H. Koh, S.B. Seo, and H.E. Kim: *Mater. Sci. Eng. C*, 2003, vol. 23, pp. 515–21.
42. H. Ji and P.M. Marquis: *J. Mater. Sci.*, 1993, vol. 28, pp. 1941–45.
43. Z. Dilshad, I. Sktani, M.M. Ratnam, and Z.A. Ahmad: *J. Aust. Ceram. Soc.*, 2016, vol. 52, pp. 167–76.
44. J. Luo and R. Stevens: *Ceram. Int.*, 1999, vol. 25, pp. 281–86.
45. A.E. Hannora: *J. Ceram. Sci. Technol.*, 2014, vol. 5, pp. 293–98.
46. V.K. Singh and B.R. Reddy: *Ceram. Int.*, 2012, vol. 38, pp. 5333–40.
47. H.R.R. Ramay and M. Zhang: *Biomaterials*, 2004, vol. 25, pp. 5171–80.
48. T.S.B. Narasaraju and D.E. Phebe: *J. Mater. Sci.*, 1996, vol. 31 (1), pp. 1–21.
49. A. Siddharthan, T.S. Sampath Kumar, and S.K. Seshadri: *Biomed. Mater.*, 2009, vol. 4, pp. 045010–19.
50. S.M. Naga, M. Sayed, H.F. El-Maghraby, and M. Awaad: *J. Mater. Sci.: Mater. in Med.*, 2018, vol. 29:55, pp. 1–10.